Heliyon 10 (2024) e32442

Contents lists available at ScienceDirect

Heliyon

journal homepage: www.cell.com/heliyon

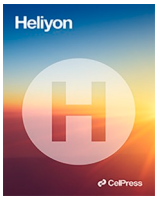

Research article

# A multi-criteria decision analysis approach for ranking the performance of CMIP6 models in reproducing precipitation patterns over Abaya-Chamo sub-basin, Ethiopia

Desalegn Laelago Ersado [a,b,*], Admasu Gebeyehu Awoke [a]

[a] School of Civil and Environmental Engineering, Addis Ababa Institute of Technology(AAiT), Addis Ababa University, Post Office Box: 1176, Addis Ababa, Ethiopia

[b] Department of Hydraulics and Water Resources Engineering, Hawassa Institute of Technology, Hawassa University, Post Office Box: 05, Hawassa, Ethiopia

ARTICLE INFO

*Keywords:*
Abaya-Chamo sub-basin
CMIP6
Multi-model ensemble (MME)
A multi-criteria decision analysis
TOPSIS

ABSTRACT

The most suitable multi-model ensemble set of general circulation models is used to reduce the uncertainty associated with GCM selection and improve the accuracy of the model simulations. This study evaluated the performance of 20 global climate models participating in the Coupled Model Intercomparison Project Phase 6 (CMIP6) in reproducing precipitation patterns over the Abaya-Chamo Sub-basin, Ethiopia. For the validation and selection of the models' capabilities, datasets from the Climate Hazards Infrared Precipitation with Stations (CHIRPS) were used after comparing them with ground observational datasets. The objective was to identify the most suitable multi-model ensemble (MME) of a subset of CMIP6 GCMs to capture the rainfall for the 1981–2014 period over the region. Climate Data Operators (CDOs) were used in climate data processing and extraction, and the Mann-Kendall test and Theil-Sen slope estimator methods were utilized to analyze the trends of the CMIP6 simulations. Four statistical metrics (Nash-Sutcliffe coefficient, percent bias, normalized root mean square error, and Kling-Gupta efficiency) were used to further assess the performance of the models. A multi-criteria decision analysis approach, namely, the technique for order preferences by similarity to an ideal solution (TOPSIS) method, was used to obtain the overall ranks of CMIP6 models and to select the best-performing CMIP6 model in the region. The results indicated that CHIRPS and most of the CMIP6 simulations generally reproduced bimodal precipitation patterns over the region. The CESM2-WACCM, NorESM2-MM, NorESM2-LM, and NorESM2-LM models performed better than the other models in reproducing seasonal patterns for the winter, spring, summer, and autumn seasons, respectively. On the other hand, FGOALS-f3-L revealed the trends of the reference datasets for all seasons. In terms of the NSE, PB, NRMSE, and KGE metrics, EC-Earth3-C, EC-Earth3, EC-Earth3-C, and EC-Earth-C, respectively, were considered good at representing the observed features of precipitation over the region. EC-Earth3-C,EC-Earth3, EC-Earth3-Veg-LR, ACCESS-CM2, MPI-ESM1-2-HR, and CNRM-CM6-1-HR exhibited the best performances in the Abaya-Chamo Sub-basin.

* Corresponding author. School of Civil and Environmental Engineering, Addis Ababa Institute of Technology(AAiT), Addis Ababa University, Post Office Box: 1176, Addis Ababa, Ethiopia.

*E-mail address:* desalegnlog@gmail.com (D.L. Ersado).

https://doi.org/10.1016/j.heliyon.2024.e32442
Received 29 December 2023; Received in revised form 30 May 2024; Accepted 4 June 2024
Available online 8 June 2024

## 1. Introduction

Developing countries are the most vulnerable to climate change due to their dependence on rain-fed agriculture subsistence, limited resilience to climate change [1].In Ethiopia, it has been observed that droughts and floods are becoming more severe and frequent as a result of climate change [2]. So far, the impact of climate change in Ethiopia were observed in terms of increasing maximum, minimum temperature and intensity of precipitation events [3], change in the runoff pattern [4,5], and frequency and magnitude of the change in precipitation intensity and flood frequency [2,6]. Therefore, assessing the potential local-scale effects of climate change with the corresponding multiple conceivable climate change scenarios is crucial to planning the water resources system.

The climate model information is the key tool for analyzing the effects of localized past climate change [7], gaining insights into potential future climate changes, and creating climate-resilient systems [1]. General circulation models (GCMs) are mostly used tools to capture relevant physical elements and processes that affect the climate system and to evaluate the impacts of climate change. Global climate models have contributed to the most recent state-of-the-art climate model experiments version, the Coupled Model Intercomparison Project Phase 6 (CMIP6) [8]. CMIP6 has a substantial improvement over the previous generations of CMIP [9] in terms of emission pathway representation, high spatial resolutions, the number of participating modeling groups, the number of different experiments conducted, and additional earth system processes and components [1,8,10]. Globally, many studies have used coupled atmosphere-ocean general circulation models to study current climate trends, and prediction of future hydrologic response scenarios globally under various greenhouse gas (GHG) emission scenarios [11–13]. Although, Various studies have been carried out over the African continent by several researchers [7,10,14–18] with the use of either general circulation models (GCMs) or regional climate models (RCMs) to assess the past and future climate change impacts.

In Ethiopia, GCM product data have been widely utilized to characterize the climate changes of different regions and, to create climate information for various applications purposes [3,19–21]. For example, in the Rift Valley lakes basin, numerous investigations have been carried out to determine the effects of climate change using the GCM and RCM output [20,22]. However, many prior regionalized studies focused haphazardly on utilizing randomly selecting GCMs/RCMs models to forecast the future climate without applying performance evaluation of models [20,23].

Performance evaluation of models is used to select the best suitable multimodel ensemble set of GCMs, compensate for individual model errors, and decrease overreliance on a single GCM output for impact studies in water resources planning [24]. Furthermore, selecting the best performance models is important for mapping present and future hotspots and extreme rainfall events [7]. The best suitable multimodel ensemble set of GCMs is used to reduce the uncertainty associated with GCM selection in the assessment of climate change impact [25]. More importantly, the effectiveness of adaptation and mitigation actions and sustainable planning for the future relies on the ability of GCM's historical outputs simulations [7]. Therefore, these justified the importance of validating the accuracy of General circulation models (GCMs) historical simulations before being applied in assessments of climate change signals at present time and projected climate change. Globally, many studies have been conducted on GCM performance evaluation in simulating the characterization of climatic variable patterns in different regions [26]. For instance, Omay [7] evaluated 23 Global climate models to identify the top best-performance models in capturing patterns of rainfall for the 1981–2014 period over the intergovernmental authority on development (IGAD) region of Eastern Africa. The simulation results of the climatic models showed variations in the performance of models within the region, basin, meteorological variables, and location levels [7]. Although, a numerous of studies have evaluated the performance of CMIP6 models in simulating climate patterns over Ethiopia [1,27–30]. [1] compared the output from the CMIP6 models simulation with observational data for the baseline period (1981–2010), and further validated the performance of MRI-ESM2-0 and BCC-CSM-2MR in predicting future climate trends in the Upper Blue Nile Basin. Berhanu [31] evaluated the performance of 37 CMIP6 models against gridded rainfall product of Ethiopia models, and GFDL-CM4 was identified as the best-performing model, followed by GFDL-ESM4, NorESM2-MM, and CESM2. The majority of CMIP6 models successfully reproduced the seasonal severe precipitation indices' spatial distribution, but they had difficulty capturing their magnitude, particularly in the country's highland and high rainfall regions. Similarly, Feyissa [29] identified multi-models ensemble (MME) with optimal performance in reproducing precipitation over the Omo basin, Ethiopia. Sime [30] evaluated the performance of CMIP6 models in simulating extreme precipitation in the Awash basin, and found that MIROC6, CESM2-WACCM, and Ensemble as well-performing models.

Therefore, the selection of representative GCM models needs strong attention during climate change impact study for a specific location, especially at small scales like sub basin. The performance of Regional Climate Model (RCM) in the Rift Valley Lakes Basin of Ethiopia has been evaluated in several studies [28,32,33]. For example, Balcha [34], conducted extensive evaluation of five RCMs from 22 GCM outputs available in the Coordinated Regional Downscaling Experiment (CORDEX)-Africa database against ground-based observed rainfall over Central Rift Valley Lakes sub basin. Kuma [33] employed the ensemble average of five regional climate models with their driving GCMs for Climate change projection over Bilate catchment, Rift valleys Lakes Basin. Similarly, Girma [28] evaluated eleven CORDEX-Africa regional climate models' performance in simulating climate variables over the Gidabo river basin, and the result shows that RACMO22T (EC-EARTH) performed well in reproducing mean annual rainfall, while CCLM4–8 (MPI) and the mean ensemble replicated annual rainfall patterns. in the Ethiopian main rift valley. Temesgen [35] conducted critically reviews on recent researchers those used CORDex-RCM model with RCP 4.5 and RCP 8.5 scenarios to evaluate the potential effects of climate change on hydro-climatic variables over Abaya-Chamo Sub-basin. These studies collectively underscore the need for further research using CMIP6 (Coupled Model Intercomparison Project Phase 6) to advance our understanding of climate processes and improve the reliability of future climate projections over the Southern Ethiopian Rift Valley catchment (Abaya-Chamo sub-basin). As far as we know, no previous research has investigated the multiple CMIP6 simulation performance analysis to evaluate the ability of the CMIP6

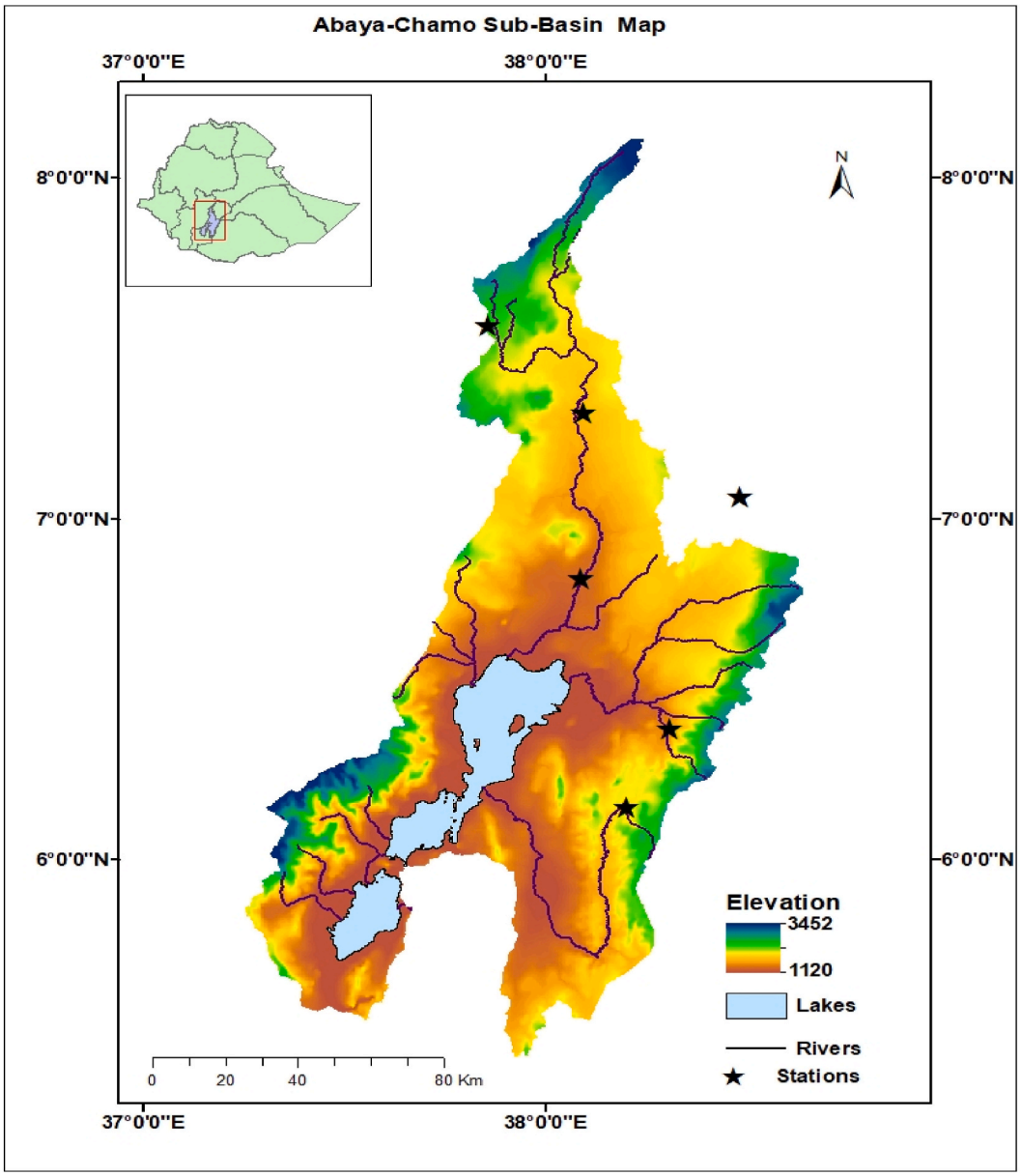


**Fig. 1.** Location map of the study area with elevation profile and meteorological stations.

outputs to reproduce the pattern of climatology variables and possible future conditions over the Abaya-Chamo sub-basin.

Consequently, this study makes use of 20 CMIP6 models to understand how future hydro climatology projections can be effectively handled with a selected top-ranked suitable multi model ensemble of CMIP6 GCMs. The study aims to identify the most suitable multi-model ensemble (MME) of a subset of CMIP6 GCMs over the Abaya-Chamo sub-basin. Due to the low density of rain gauge networks over the region, Climate Hazards Infrared Precipitation with Stations (CHIRPS) datasets product have been used as proxies for observational datasets to evaluate the quality of climate models in reproducing precipitation. In this study, multi-criteria decision-making techniques based on statistical and categorical metrics and trend analysis methods were used to rank multiple CMIP6 GCMs. The results of this study are intended to be used by policymakers to study the impact assessment of climate change on hydrology to support decision-making and inform climate adaptation and mitigation strategies over the Abaya-Chamo sub-basin.

## 2. Materials and methods

### 2.1. Study area

The Abaya-Chamo subbasin is located in the Southern part of Ethiopia in the Rift Valley Lakes Basin between latitudes 5° 52 'N and 8°8' N, and longitudes 37° 16 'E and 38°39.5' E with a total drainage area of about 18,600 $km^2$, including freshwater bodies (Fig. 1). The region's topographic altitudes range from 1120 masl to 3452 m.a.s.l. The sub basin has encompassed Nech Sar National Park and two hydrologically interconnected lakes, Abaya and Chamo Lakes. The main rivers that drain into the Abaya lakes include the Gelana, Bilate, Gidabo, Hare, Baso, and Amessa Rivers. whereas Sile, Argoba, Wezeka, and Sego overflow from Lake Abaya confluence with the Kulfo Rivers are draining into the Chamo Lake [36].

The areas around Lake Chamo and the southern part of Lake Abaya exhibit a bimodal precipitation pattern from March to May (MAM) and September to October. Whereas, in the northern part of Lake Abaya, the precipitation seasons are July to October and March to April [37]. In the subbasin, mean annual precipitation and temperature ranged from 665 to 1240 mm and 8.8 $^{\circ}$C to 31.2 °C, respectively [38].

### 2.2. Observed data sets

The observed meteorological data used for validation of reanalysis observed data. Available ground historical daily observed precipitation data series were collected from the Ethiopian National Meteorological Agency (NMA). More than 16 weather observation stations within and around the Abaya-Chamo Sub-basin were analyzed. However, the observed data records are often incomplete due to missing observed data in the measured period. The common problems of the observed climatic variable are missing data, sparse distribution of rain gauges, and insufficient long-term records of climatic observation [39]. Daily precipitation data sets with no missing values are required for efficient estimation for application purposes [40]. Therefore, the inverse distance method (IDM) was used to fill in the missing precipitation records based on the distance between the target station and the nearby stations. Hence, six stations, namely Dilla, Yirgachafe, BilateTena, Halaba Kulito, Hossana, and Hawassa were selected to represent the climatic condition of the study areas. These stations were chosen because of the location of the station with higher-quality data and temporal coverage. Therefore, the average monthly observed precipitation distribution of six stations was used to evaluate monthly mean of the Reanalysis dataset results.

The high resolution of spatial-temporal observed data is extremely important to understanding meteorological and hydrological investigation and the consequence of future climate variation at the basin and sub-basin level [29]. Reanalysis product provides optimized comprehensive and coherent global climate datasets for representing the climatology information and their inter-annual variability in the historical periods [41,42]. The Climate Hazard Group Infrared Precipitation with Stations (CHIRPS) was validated and evaluated in different regions of Ethiopia and showed high performance over others [43,44]. Therefore, considering the improvement of the spatiotemporal resolution, CHIRPS reanalysis gets more attention to the value of precipitation reanalysis data in climate and hydrology analysis [45]. Therefore, the most recent version of the CHIRPS dataset with a spatial resolution of 0.05° x 0.05° and a daily timescale was used in this study for trend analysis and CMIP6 performance evaluations. This data set is freely downloaded from (ftp://ftp.chg.ucsb.edu/pub/org/chg/products/CHIRPS-2.0/) (accessed on August 16, 2022).

### 2.3. CMIP6 GCMs model datasets

The simulations of the CMIP6 climate model's data were downloaded from Earth System Grid Federation (ESGF) archive (https://esgf-node.llnl.gov/search/cmip6/). A total of this study uses 20 daily historical simulations of CMIP6 models that participated in the new Sixth Phase of CMIP6 [8]. A total of 20 CMIP6 GCM simulations have been evaluated to reproduce the precipitation in this study area. Details of the models used in this study are summarized in Table (Appendix). The choice of the model outputs was based on their better performance in East Africa and South Asia and Middle East North Africa [15,16] and Ethiopia [1], the availability of the socioeconomic pathways (SSPs), the availability of daily and monthly simulation predictor data at the time of the analysis. The daily precipitations data of all selected model simulation were changed into monthly mean, annual mean and seasonal mean series using CDO statistical values analysis commands [46]. These data can also be used to evaluate how well models simulate spatial and temporal patterns of climate variables across different region.

Multi-model ensemble set GCMs are often employed to reduce the uncertainties and biases related to GCM simulations, to avoid the weaknesses associated with Models and improve the accuracy of climate projections. In this study, CMIP6 multi-model ensemble has been evaluated for its performance in simulating observed data. The multi-model ensembles (MMEs) set of GCM was generated by averaging all selected individual GCMs models using a simple arithmetic mean technique based on Equation (1):

$$\mathrm{MME} = \frac{1}{n}\sum_{i=1}^{n} \mathrm{GCM}_{si} \tag{1}$$

Where, n is number of GCMs considered, GCMsi is interpolated precipitation values of models.

### 2.4. GCMs outputs grid interpolation and extraction

The CMIP6 GCM selected for this study comes with a variety of spatial resolutions (typically between 2.8° x 2.8°and 0.5° × 5°). Therefore, before performance evaluation to facilitate the inter comparison between models, all models outputs and observational data were interpolated into the GCM the finest spatial resolutions of 0.5° × 5° using interpolation methods. The common types of interpolation techniques used in GCM are inverse distance weighting (IDW), bilinear interpolation, bicubic interpolation, and kriging interpolation methods. Therefore, in this study, bilinear interpolation methods of the Climate Data Operators (CDO) were used for precipitation remapping. We used the Climate Data Operators version 2.0.5 (https://code.mpimet.mpg.de/projects/cdo) software [46] from the Max Planck Institute. Climate Data Operators (CDOs) represent a set of statistical and arithmetic commands useful for climate atmospheric data processing in NetCDF and GRIB format, spatial interpolation, data selections, and subsampling tools [46].

### 2.5. Trend analysis methods

The significant trend analysis test in the climatologic time series can be done using parametric and non-parametric approaches [47,48]. Parametric trend test approaches require data to be independent and normally distributed, whereas, non-parametric trend test approaches make no assumptions about the underlying distribution of the data and the test has low sensitivity to abrupt breaks due to inhomogeneous time series [49]. In this study, non-parametric trend analysis methods namely, the Mann-Kendall test and Theil-Sen Slope Estimator methods were utilized to find potential trends in the observed datasets, reanalysis model simulation trends, and CMIP6 simulations.

#### 2.5.1. Mann-Kendall trend test

The Mann-Kendall statistical test (Mann, 1945; Kendall, 1975) has been used extensively to evaluate the significance of trends in hydro meteorological time series and is a commonly adopted and favored method over other non-parametric tests [47,49–51]. In the context of CMIP6, Mann-Kendall test is applied to assess trends in model output for variables of interest across different models and scenarios. It has been widely used in the evaluation of precipitation trends observed in historical data or projected trends under different future scenarios [52]. The Mann-Kendall test statistic(S) is calculated as (Equation (2)):

$$S = \sum_{i=1}^{n-1} \sum_{j=i+1}^{n} sign(xj - xi) \tag{2}$$

$$sign(xj - xi) = \begin{Bmatrix} 1, \text{if } (xj - xi) > 0; \\ 0, \text{if}(xj - xi) = 0; \\ -1, \text{if}(xj - xi) < 0; \end{Bmatrix}$$

Where, $n$ is the number of data points, $xi$, and $xj$ are the annual data values in the time series $i$ and $j$ ($j > i$), respectively and sign ($xj-xi$) is the sign function assigned the integer value of 1, 0, or −1.

If a number of sample data sizes are greater than 10 (n > 10), the standard normal test statistic ($Z_S$) is computed using the S – statistics (Equation (2)) and variance (Equation (3)).

The variance is computed as (Equation (3)):

$$Var(S) = \frac{n(n-1)(2n+5) - \sum_{i=1}^{m} t_i(t_i-1)(2t_i+5)}{18} \tag{3}$$

Where, $n$ is the number of data points, $m$ is the number of tied groups and $t_i$ denotes the number of ties of extent $i$, the summation sign (Σ) indicates the summation over all tied groups. A tied group is a set of sample data having the same value.

The standard normal test statistic $ZS$ is computed using Equation (4):

$$Z_S = \begin{Bmatrix} \frac{S-1}{\sqrt{Var(S)}}, if\ S > 0 \\ 0, \text{if } S = 0; \\ \frac{S+1}{\sqrt{Var(S)}}, if\ S < 0 \end{Bmatrix} \tag{4}$$

Positive values of $Z_S$ indicate increasing trends while negative $Z_S$ values show decreasing trends. When $|Z_S| > Z_{1-\alpha/2}$ , the Null hypothesis is rejected and a significant trend exists in the time series. $Z_{1-\alpha/2}$ is obtained from the standard normal distribution table (https://www.z-table.com/). For making statistical decision, testing trends is done at the specific significance level of 5 % [53].

#### 2.5.2. Sen's slope estimation methods

Sen's slope estimation method can be applied to assess trends climatic variables simulated by climate models and compare them with observed trends from historical data [54]. Sen's [55], methods are used to detect the magnitude of the trend and estimate the overall slope of precipitation time series data. The slope of all data pairs is computed as (Equation (5)):

$$T_i = \frac{(x_j - x_k)}{j - k} \; for \; i = 1, 2, 3 \ldots N \tag{5}$$

Where $x_j$ and $x_k$ are the data values at times j and k (j > k) respectively.

For a time series $x$ having $n$ observations, there is a possible $N = \frac{n(n-1)}{2}$ values of $T_i$ that can be calculated. According to Sen's method, the overall estimator of the slope is the median of these N values of Ti. The overall slope estimator $Qi$ is thus:

Qi $= T_{(N+1)/2}$ for N odd observation

$= \frac{1}{2}(T_{N/2} + T_{(N+2)/2}$ For N even observation

In this study, both Mann-Kendall test statistics and Sen's test values were calculated by using XLSTAT (2015.5.01) (https://www.xlstat.com). XLSTAT is a data analysis system for Microsoft Excel that allows users to explore, visualize, and model their data. The system contains a comprehensive set of features that include data preparation, exploration through machine learning (ML), and data visualization through charts, graphs, and diagrams.

### 2.6. Model evaluation metrics

The spatiotemporal performance skill of the 20 bias-corrected CMIP6 models over the Abaya-chemo sub-basin against the CHIRPS were evaluated through statistical metrics. The statistical metrics used for validation and verification purposes of CMIP6 precipitation simulations against observations datasets are the Nash-Sutcliffe coefficient (NSE), percent bias (PB), normalized root mean square error (NRMSE), and Kling–Gupta efficiency (KGE). The statistical evaluation metrics are defined in equations (6)–(9).

$$NSE = \left[ \frac{\sum_{i=1}^{n} \left(Y_i^{obs} - Y_{obs}^{mean}\right)\left(Y_i^{sim} - Y_{sim}^{mean}\right)}{\sum_{i=1}^{n} \left(Y_i^{obs} - Y_{obs}^{mean}\right)^2 \sum_{i=1}^{n} \left(Y_i^{sim} - Y_{sim}^{mean}\right)^2} \right] \tag{6}$$

$$PB = \left[ \frac{\sum_{i=1}^{n} \left(Y_i^{obs} - Y_i^{sim}\right) * 100}{\sum_{i=1}^{n} Y_i^{obs}} \right] \tag{7}$$

$$NRMSE = \frac{\sqrt{\left[\frac{1}{n}\sum_{i=1}^{n} \left(\left(Y_i^{obs} - Y_i^{sim}\right)^2\right]\right.}}{Xmax - Xmin} * 100 \tag{8}$$

Where, $Y_i^{obs}$ *and* $Y_i^{sim}$ are the observed and simulated values, respectively; $Y_{obs}^{mean}$ is the mean of observed data for the constituent being evaluated, $Y_{sim}^{mean}$ is the mean of simulated data, $x_{max}$ and $x_{min}$ are the maximum and minimum values of observed data and $n$ is the number of target data used for testing.

The KGE is an objective statistical metric [56] with multiple-component nature of assessment, and developed for the model performance assessment. KGE considers three statistical measures namely; Pearson correlation, variability ratio, and bias ratio. KGE values can range between -∞ and 1, where values close to 1 are preferred.

$$KGE = 1 - \sqrt{\left(\alpha_p - 1\right)^2 + \left(\beta_p - 1\right)^2 + \left(\gamma_{RP} - 1\right)^2} \tag{9}$$

Where $\alpha_p$ the Pearson correlation between observed and GCM-simulated data is, $\beta_p$ is the bias ratio, and $\gamma_{RP}$ is the variability ratio. Equations (10) and (11) show the calculation of $\beta_p$ and $\gamma_{RP}$ respectively.

$$\beta_p = \frac{\mu_G}{\mu_O} \tag{10}$$

Where, $\mu_G$ and $\mu_O$ refer to the mean of GCM-simulated and observed data respectively.

$$\gamma_{RP} = \frac{CV_G}{CV_O} = \frac{\frac{\alpha_G}{\mu_G}}{\frac{\alpha_O}{\mu_O}} \tag{11}$$

Where $CV_G$ and $CV_O$ refer to the coefficient of variation of GCM-simulated and observed data respectively.

In this study, the Kling–Gupta efficiency (KGE) values for climatic models and reference datasets are calculated using Agrimetsoft online calculator tools (https://agrimetsoft.com/calculators).

### 2.7. Multiple-criteria decision-making (MCDM) techniques

The ranking and selection of multiple GCMs become more challenging when multiple model performance measures are used with

multiple climate variables. In such a case, an information aggregation approach (IGA) that combines information from several model performance measures can be used. GCMs' performances for mean precipitation were first ranked individually using four spatial performance measures, and then the overall ranking scores of the GCMs' performances were calculated using ranking scores of the GCMs' performances by multiple spatial performance measures [13].

In this study, a multi-criteria decision analysis approaches, namely the technique for order preferences by similarity to an ideal solution (TOPSIS) methods were used to obtain the overall ranks of 20 CMIP6 models and select the best performing CMIP6 in the Abaya-chemo sub-basin. The TOPSIS technique is a multi-criteria decision-making approach for sorting alternatives based on the shortest distance from the positive ideal solution (PIS) and the furthest distance from the negative ideal solution (NIS) [57,58].

Considering a set of alternatives $A_k$, $k = 1 \ldots$, n, a set of criteria $C_j$, $j = 1 \ldots$ m, the matrix $x_{kj}$ is the performance ratings of alternative k to criteria j, and $\omega_j$ is the original weight given to each criterion. In this study, the selected number of CMIP6 GCMs precipitation values are alternatives and a set of statistical metrics were considered as criteria. Therefore, the TOPSIS method is deployed in the following steps [57].

Step1 Normalization of performance ratings Matrix, $r_{kj}(x)$

➢ For criteria to maximize (the larger, the better), the normalized rating ($r_{kj}$) is given by:

$$r_{kj}(x) = \frac{x_{kj} - x_j^-}{x_j^* - x_j^-}, k = 1, \ldots, n; j = 1, \ldots, m,$$

➢ For criteria to minimize (the smaller, the better), the normalized rating ($r_{kj}$) is given by:

$$r_{kj}(x) = \frac{x_j^- - x_{kj}}{x_j^- - x_j^*}, k = 1, \ldots, n; j = 1, \ldots, m,$$

Where $x_j^*$ is the desired level of criteria j and $x_j^-$ is the worst level

Step 2 Formation of a weighted Normalized Decision matrix, $U_{kj\ (x)}$:

$$U_{kj\ (x)=}\ \omega_j r_{kj}(x), k = 1, \ldots . n;\ j = 1, \ldots ., m.$$

Step 3 Derivation of positive ideal alternatives (Ap) and negative ideal alternatives (An):

Positive ideal alternatives and negative ideal alternatives represent the more preferable and the less desired set of criteria one wishes to achieve respectively. Ap and An are given by:

$$A_p = \left\{ \left({}_k^{max} Ukj\ (x)\ \ \backslash j \in j_1 \right), \left({}_k^{min} Ukj\ (x)\ \ \backslash j \in j_2 \right), k = 1, \ \ldots, \ n \right\}$$

$$A_n = \left\{ \left({}_k^{min} Ukj\ (x)\ \ \backslash j \in j_1 \right), \left({}_k^{max} Ukj\ (x)\ \ \backslash j \in j_2 \right), k = 1, \ \ldots, \ n \right\}$$

Where $j_1$ and $j_2$ are the benefit and cost elements respectively.

Step 4 Calculate the alternative distance from $A_p$ and the $A_n$.

The separation from the Ap, $D_a$+and the $A_n$, $D_a{}^-$ can be estimated as Euclidean distance formula:

$$D_a^+ = \sqrt{\sum_{j=1}^{m} \left[ Ukj\ (x) - U_j^+(x) \right]^2}, k = 1 \ldots n$$

$$D_a^- = \sqrt{\sum_{j=1}^{m} \left[ Ukj\ (x) - U_j^-(x) \right]^2}, k = 1 \ldots n$$

Where, $U_j^+(x)$ *and* $U_j^-(x)$ are positive and negative ideal values of criterion j, respectively.

Step 5 Derivation of A multi-criteria performance rank score

The similarities to the Ap are computed as $(C_k^+)$:

$$C_{k=}^+ \ \frac{D_a^-}{D_a^+ + D_a^-}, k = 1 \ldots ., n$$

Finally, the alternatives can be ranked from most preferred to less prefer by ordering $C_k^+$ in decreasing order. Hence, the results of the performance indicators of different timeframes are integrated into one and arranged in descending order to rank GCMs for the

individual climate variable ranking.

## 3. Results and discussion

### 3.1. Annual cycle

The performance of 20 CMIP6 models is examined based on their capability to mimic regional mean annual climatology and seasonal variability. The results revealed that the observed long-term spatiotemporal trends of precipitation of the study region of the annual dataset in the Abaya-Chamo sub-basin are mostly characterized by bimodal precipitation patterns with maximum precipitation from March to May and from September to November (as shown in Fig. 2). The observed monthly mean precipitation of all stations shows decreasing trends during September, October, November, December, April, May, and June, and all station has increasing trends in February, March, April,. The observed annual peak mean precipitation is 7.65 mm in April, and the lowest amount was found between December and January (0.45 mm). Hence, the main precipitation seasons of the region are March April, and May (MAM), followed by a lesser precipitation season from October to January.

Based on Climate Hazard Group Infrared Precipitation with Stations (CHIRPS) datasets analysis results, the precipitation pattern over the region is primarily described as bimodal, with the highest precipitation mostly occurring during the middle of Spring (MAM) season to Summer (JJA) season, and moderate precipitation up to the middle of autumn season (SON). Whereas, the lowest precipitation is categorized from the end of autumn to the whole winter season (DJF). The highest amount recorded during the annual cycle was 5.24 mm in April, and the lowest amount was 0.85 mm between December and January. The average monthly observed precipitation distribution of six stations and monthly mean of CHIRPS datasets depict almost similar patterns with a slight difference for April–May and September–October. The bimodal pattern of the region is associated with the regional and global change of the weather systems, the complex topographical variations, and the Inter-Tropical Convergence Zone (ITCZ) passes through the region to its southern position [59].

Therefore, the ability of each CMIP6 model and model ensemble to mimic the yearly precipitation cycles of CHIRPS datasets were presented in Fig. 3. More than 80 % of the models' simulations accurately reflect bimodal precipitation patterns, and the low and peak precipitation were adequately approximated by a few GCM models and the ensemble mean over the region. The BCC-CSM2-MR, CESM2-WACCM, NESM3, EC-Earth3-Veg-LR, ACCESS-ESM1-5, MIROC6, and FGOALS-g3 perform relatively poorly as they do not reproduce observed bimodal precipitation pattern. However, some models somewhat overestimated and underestimated the amount of precipitation during the low and high precipitation seasons of the reference datasets. The ensemble mean performs best from October to April, and for the rest of the year, it tends to overestimate observed precipitation and CHIRPS. The multi-model mean (MME) ensemble is not adequately reproducing the observed features from June to August (JJAS). This is similar to previous studies [7] in East Africa that CMIP MME did not perform better than the individual models in simulating JJAS precipitation over the Ethiopia.

### 3.2. Seasonal patterns of precipitation

Accessing specific simulated seasonal mean precipitation values from the CMIP6 dataset is used to understand know how different climate factors influence precipitation variability on seasonal time scales and to compare with observed data seasonal values. The monthly values for each seasons were averaged to obtain seasonal precipitation for each of the observed precipitation stations, reanalysis datasets, and 20 CMIP6 models. According to Ethiopia's seasonal basis, the entire year is divided into four seasons: Belg (autumn), Kiremt (summer), Tseday (spring), and Bega (winter). The summer (JJA), spring (SON), autumn (MAM) and winter (DJF)

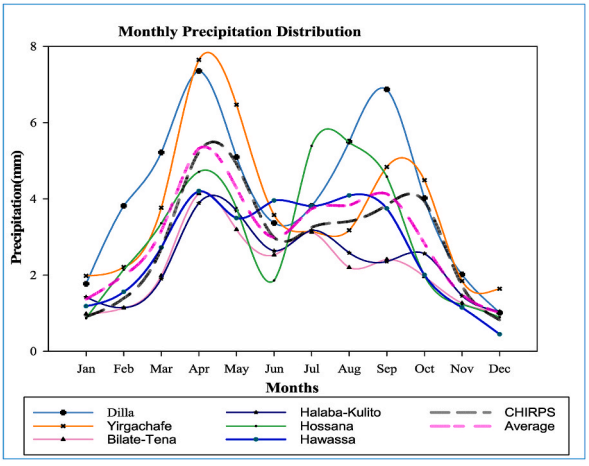


**Fig. 2.** Annual cycle of mean monthly precipitation (mm/month) over Abaya-Chamo sub-basin on selected stations, average monthly precipitation over sub-basin and alongside CHIRPS datasets.

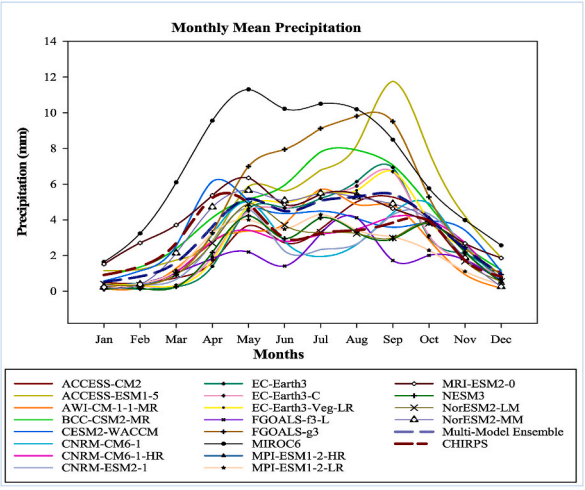


**Fig. 3.** Annual cycle of long-term mean monthly precipitation (mm) over the Abaya-Chamo Sub-basin, averaged between longitudes 37° E to 39° E and latitudes 5° N and 9° N, for the period 1981–2014. The ensemble mean and CMIP6 models are compared against CHIRPS. CHIRPS is represented by the long-short line type, and the multi-model ensemble is represented by the long-long line type.

seasons are categorized as heavy rain falls months, harvest months, dry with frost in the morning months and hottest months respectively. The Bega seasons (the dry seasons) occur from mid-October to January and are characterized by low precipitation patterns. The maximum precipitation pattern is categorized from mid of the MAM to the end of the JJA. These seasonal precipitation variation in Ethiopia are mainly driven by the migration of the Inter-Tropical Convergence Zone (ITCZ) as main driver of simulated and projected precipitation over the region [60], and Earth's orbit around the Sun and its axial tilt relative to the ecliptic plane [61] and the influence of Gulf of Guinea, southern Pacific and northern Atlantic oceans [62].

The seasonal patterns of CMIP6 models simulation results show enhanced precipitation over Summer Season (JJA). Conversely, models that exemplify unsatisfactory performance over the JJA season include CNRM-ESM2-1, CNRM-CM6-1, and FGOALS-f3-L models. Remarkably, in the Spring (MAM) and Winter (DJF) seasons, more than 80 percent of the CMIP6 model's precipitation simulation depicted a pronounced underestimation of the CHIRPS precipitation simulation and observed precipitation. Overall, comparatively, the best-performing models in the Winter (DJF) seasonal precipitation simulations over the region are CESM2-WACCM and ACCESS-ESM1-5. Similarly, NorESM2-MM and BCC-CSM2-MR model simulations are the best-performing models in the spring (MAM) season. Whereas, NorESM2-LM and CNRM-CM6-1-HR models simulation performed relatively better than other models in reproducing the reanalysis and observed data in the summer (JJA) season over the region. Nearly 4 out of 20 models namely, NorESM2-LM, MRI-ESM2-0, CESM2-WACCM, and CNRM-ESM2-1 models simulation performed relatively better than other models in reproducing the Autumn (SON) season precipitation over the region, whereas 4 models slightly underestimate the seasonal rain pattern (Fig. 3).

### 3.3. Trend analysis

The trends were evaluated and tested for their significance and magnitude over Abaya-Chamo during 1981–2014. The statistical tests result of the linear trend of mean historical precipitation for annual and all seasons over the period 1981–2014 are presented in Table 1. The precipitation simulation of models over the region exhibits decreasing, and increasing trends and no significant change. CHIRPS depicts increasing trends for the annual, SON, MAM, and JJA seasons, and a significant decreasing trend with Z-score values of −0.105 during the DJF season. These annual trend test results agree with past studies in the study area [61]. Although Ethiopia's central Rift Valley region are mostly experienced mixed trends of precipitations [63,64].

The ability of CMIP6 model simulations to reproduce the trends of CHIRPS simulations varies from one model to another. The rainfall analysis of the reference datasets (CHIRPS) during annual basis shows significant increasing trends. Most of the models, i.e. more than 68 % of simulated CMIP6 models shows increasing trends during annual periods. However, models, namely NorESM2-MM, NorESM2-LM, MPI-ESM1-2-LR, NESM3, MPI-ESM1-2-LR, CNRM-CM6-1-HR and CNRM-CM6-1 reveals decreasing trends for annual precipitation. Comparatively, six models namely BCC-CSM2-MR, MRI-ESM2-0, FGOALS-g3, EC-Earth3-Veg-LR, EC-Earth3-C, and MPI-ESM1-2-MR, reproduce positive linear trends with Z– Statistics values of 0.113–0.425 within the proximity trends of CHIRPS data of 0.287. Examination of the magnitude of the slope of annual CMIP6 simulation using Sen's slope shows the capability of most models in reproducing observed CHIRPS trends satisfactorily.

The Sen's slope (Q) of FGOALS-g3, EC-Earth3-Veg-LR, BCC-CSM2-MR, MRI-ESM2-0, EC-Earth3-C, MPI-ESM1-2-MR, and ACCESS-ESM1-5 were 0.014, 0.022, 0.026, 0.003, 0.008, 0.005, and 0.006, respectively, which give increasing slope magnitude. Therefore, BCC-CSM2-MR, FGOALS-g3, EC-Earth3-Veg-LR, EC-Earth3-C, and MPI-ESM1-2-MR give significant increasing trend due to positive value of Z and Q statistics. Whereas NorESM2-MM, NorESM2-LM, MPI-ESM1-2-LR, NESM3, MPI-ESM1-2-LR, CNRM-CM6-1-HR, and

**Table 1**
Mean value, Modified Mann-Kendall trends, and Sen Slope values of Annual and all season over Abaya-Chamo Sub-basin during 1981–2014 using CHIRPS against CMIP6 models.

| Models | Test | Annual | SON | MAM | JJA | DJF |
|---|---|---|---|---|---|---|
| **CHIRPS** | Mean | 2.906 | 9.269 | 12.823 | 9.501 | 3.221 |
| | Z-score | 0.287 | 0.301 | 0.073 | 0.23 | −0.105 |
| | Slope | 0.013 | 0.092 | 0.04 | 0.056 | −0.014 |
| **ACCESS-CM2** | Mean | 2.526 | 3.688 | 3.731 | 2.015 | 0.668 |
| | Z-score | 0.069 | −0.032 | 0.072 | 0.187 | −0.045 |
| | Slope | 0.004 | −0.397 | 0.008 | 0.016 | −0.003 |
| **ACCESS-ESM1-5** | Mean | 4.917 | 7.929 | 3.472 | 6.852 | 1.406 |
| | Z-score | 0.082 | 0.062 | −0.008 | 0.022 | 0.247 |
| | Slope | 0.006 | 0.017 | −0.002 | 0.005 | 0.019 |
| **AWI-CM-1-1-MR** | Mean | 2.58 | 2.883 | 2.489 | 4.779 | 0.17 |
| | Z-score | 0.041 | 0.041 | −0.054 | 0.067 | 0.167 |
| | Slope | 0.002 | 0.003 | −0.003 | 0.008 | 0.014 |
| **BCC-CSM2-MR** | Mean | 4.269 | 4.822 | 3.892 | 3.21 | 1.13 |
| | Z-score | 0.365 | 0.197 | 0.24 | 0.024 | 0.25 |
| | Slope | 0.026 | 0.025 | 0.035 | 0.006 | 0.019 |
| **CESM2-WACCM** | Mean | 3.366 | 3.628 | 4.59 | 4.304 | 0.958 |
| | Z-score | 0.025 | −0.018 | 0.062 | −0.045 | −0.183 |
| | Slope | 0.003 | −0.002 | 0.023 | −0.007 | −0.016 |
| **CNRM-CM6-1** | Mean | 2.453 | 3.861 | 3.041 | 2.456 | 0.457 |
| | Z-score | −0.136 | −0.167 | −0.035 | −0.055 | −0.146 |
| | Slope | −0.013 | −0.566 | −0.006 | −0.005 | −0.006 |
| **CNRM-CM6-1-HR** | Mean | 2.399 | 3.632 | 2.422 | 3.15 | 0.392 |
| | Z-score | −0.244 | 0.015 | −0.166 | −0.129 | 0.029 |
| | Slope | −0.015 | 0.001 | −0.021 | −0.013 | 0.002 |
| **CNRM-ESM2-1** | Mean | 2.3 | 3.729 | 2.67 | 2.406 | 0.39 |
| | Z-score | 0.012 | −0.052 | −0.116 | 0.217 | 0.049 |
| | Slope | 0.001 | −0.011 | −0.015 | 0.02 | 0.001 |
| **EC-Earth3** | Mean | 2.951 | 4.022 | 2.09 | 5.335 | 0.355 |
| | Z-score | 0.072 | −0.126 | 0.153 | 0.123 | 0.052 |
| | Slope | 0.004 | −0.019 | 0.015 | 0.012 | 7.33E-04 |
| **EC-Earth3-C** | Mean | 2.973 | 3.867 | 2.257 | 5.319 | 0.447 |
| | Z-score | 0.119 | 0.24 | −0.055 | −0.018 | 0.045 |
| | Slope | 0.008 | 0.032 | −0.007 | −0.003 | 0.002 |
| **FGOALS-f3-L** | Mean | 1.702 | 1.826 | 1.685 | 2.913 | 0.385 |
| | Z-score | 0.062 | 0.062 | 0.055 | 0.022 | −0.018 |
| | Slope | 0.003 | 0.005 | 0.008 | 0.004 | −2.66E-04 |
| **FGOALS-g3** | Mean | 4.733 | 5.744 | 3.734 | 8.951 | 0.5 |
| | Z-score | 0.203 | 0.113 | −0.092 | 0.227 | 0.059 |
| | Slope | 0.014 | 0.021 | −0.007 | 0.037 | 0.002 |
| **MIROC6** | Mean | 7.086 | 6.08 | 8.981 | 10.297 | 2.492 |
| | Z-score | 0.026 | 0.005 | −0.15 | 0.039 | −0.351 |
| | Slope | 0 | 9.14E-04 | −0.024 | 0.005 | −0.079 |
| **MPI-ESM1-2-MR** | Mean | 2.439 | 2.894 | 2.399 | 4.282 | 0.18 |
| | Z-score | 0.133 | −0.032 | 0.126 | 0.076 | 0.207 |
| | Slope | 0.005 | −0.002 | 0.009 | 0.011 | 0.003 |
| **MPI-ESM1-2-LR** | Mean | 2.248 | 2.145 | 2.805 | 3.731 | 0.31 |
| | Z-score | −0.123 | −0.133 | 0.096 | −0.247 | 0.163 |
| | Slope | −0.004 | −0.01 | 0.006 | −0.023 | 0.005 |
| **MRI-ESM2-0** | Mean | 4.035 | 3.733 | 5.141 | 5.236 | 2.037 |
| | Z-score | 0.163 | −0.013 | 0.067 | 0.347 | 0.203 |
| | Slope | 0.003 | −0.02 | 0.005 | 0.032 | 0.007 |
| **NorESM2-LM** | Mean | 2.378 | 2.828 | 2.845 | 3.411 | 0.418 |
| | Z-score | −0.015 | −0.072 | 0.089 | −0.126 | −0.082 |
| | Slope | −0.001 | −0.012 | 0.018 | −0.019 | −0.003 |
| **NorESM2-MM** | Mean | 3.319 | 3.581 | 4.165 | 5.277 | 0.294 |
| | Z-score | −0.01 | 0.113 | 0.002 | −0.126 | −0.008 |
| | Slope | −5.71E-04 | 0.015 | 9.50E-05 | −0.018 | −1.38E-04 |
| **EC-Earth3-Veg-LR** | Mean | 3.139 | 4.365 | 2.271 | 5.382 | 0.527 |
| | Z-score | 0.425 | 0.321 | 0.106 | 0.207 | 0.227 |
| | Slope | 0.022 | 0.056 | 0.015 | 0.014 | 0.01 |

CNRM-CM6-1 give significant decreasing trend due negative values of Z and Q statistics.

The performance of a trend statistics for individual CMIP6 models in representing the seasonal trend of precipitation across the entire region was evaluated and compared with trends of reference dataset (Table 1). The seasonal CHIRPS variability for SON, MAM and JJA showed increasing trends, whereas for DJF, there was a decreasing rainfall distribution pattern over the observed period. These results are in agreement with the findings of Belay et al. [63], who examined climate variability and trends in Southern Ethiopia

and noted that the trends of seasonal precipitations had increasing and decreasing trends.

The simulated precipitation over the region shows increasing and decreasing trends in all seasons. ACCESS-ESM1-5, AWI-CM-1-1-MR, and FGOALS-g3 showed increasing trends during SON, JJA, and DJF seasons. However, three models, EC-Earth3-Veg-LR, BCC-CSM2-MR, and AWI-CM-1-1-MR show increasing trends over all seasons. On other hand, FGOALS-f3-L reveals the trends of reference datasets (CHIRPS) in all seasons. Both FGOALS-f3-L and CHIRPS showed increasing trends annually and in all seasons, expect for DJF seasons. During SON season, EC-Earth3-Veg-LR, EC-Earth3-C, FGOALS-g3, and NorESM2-MM showed increasing trends, with ranges of 0.321, 0.240, 0.062, and 0.113 respectively. However, at MAM season, ACCESS-CM2, BCC-CSM2-MR, CESM2-WACCM, EC-Earth3, FGOALS-f3-L, MPI-ESM1-2-MR, MPI-ESM1-2-LR, NorESM2-LM and EC-Earth3-Veg-LR showed increasing trends similar with reference dataset trends. Although ACCESS-CM2, ACCESS-ESM1-5, BCC-CSM2-MR, CNRM-ESM2-1, EC-Earth3, FGOALS-f3-L, FGOALS-g3, MIROC6, MPI-ESM1-2-MR, and EC-Earth3-Veg-LR shows increasing trends in the JJA seasons. Although during Winter (DJF) season NorESM2-LM, ACCESS-CM2, CESM2-WACCM, CNRM-CM6-1, FGOALS-f3-L, MIROC6, and NorESM2-MM showed decreasing trends over the Abaya-Chamo Sub-basin.

Over all, it was found that there is significant variation in CMIP6 simulations and CHIRPS reanalysis data sets over seasons and annually. The MK trend test showed that there was a statically significant increasing trend for the EC-Earth3-Veg-LR, BCC-CSM2-MR, and AWI-CM-1-1-MR over the whole seasons. The trend analysis of mean SON precipitation showed the highest increasing trend for EC-Earth3-Veg-LR with Z (0.321), followed by EC-Earth-C with Z (0.24). A significant decreasing trend was observed for the CNRM-CM6-1, CESM2-WACCM, ACCESS-CM2, CNRM-CM6-1-HR, CNRM-ESM2-1 and EC-Earth-3 models during SON season.in contrast, a large number (37 %) of CMIP6 models, namely NorESM2-LM, MPI-ESM1-2-LR, FGOALS-f3-L, EC-Earth3, MRI-ESM2-0, CESM2-WACCM, BCC-CSM2-MR and ACCESS-CM2 exhibited increasing trends in the autumn (MAM) season (Table 1). Therefore, the first top-five models that predict annual observed data trends were BCC-CSM2-MR, FGOALS-g3, EC-Earth3-Veg-LR, EC-Earth3-C, and MPI-ESM1-2-MR. EC-Earth-Veg-LR, EC-Earth-C, BCC-CSM2-MR, FGOAL-g3, and NorESM2-MM models attempt to predict the historical trends of SON seasons of the region. The observed increasing and decreasing trends of precipitations may be caused by atmospheric-oceanic mechanisms that affect rainfall in the region, Inter-Tropical Convergent Zone (ITCZ), and the dynamics of global warming caused by El Niño Southern Oscillation (ENSO) which is a natural climate phenomenon variation in East Africa [63,64].

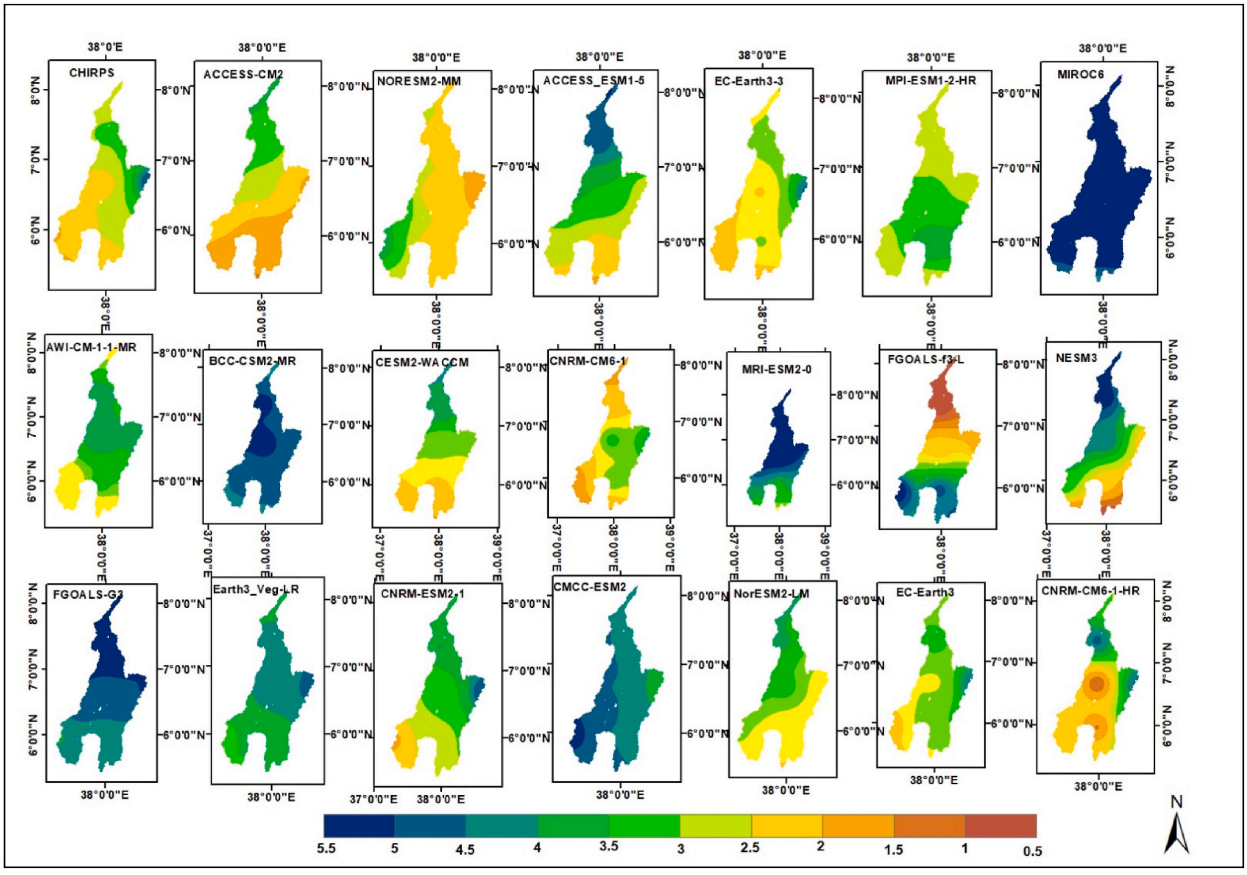


**Fig. 4.** Spatial distribution of mean precipitation during the MAM season for 20 CMIP6 models and CHIRPS over the Abaya-Chamo Sub-basin from 1981 to 2014.

### 3.4. Spatial distributions of CMIP6 performances

The spatial distribution of average rainfall during the MAM season from 20 CMIP6 models, relative to observational reference datasets (CHIRPS v2.0) for the period 1981–2014, is presented in Fig. 4. The models generally capture the spatial pattern of average rainfall in the southern and eastern parts of the region during the MAM season. For example, the CNRM-CM6-1, CNRM-ESM2-1, EC-Earth3-C, CESM2-WACCM, ACCESS-ESM1-5, and ACCESS-CM2 models simulate rainfall distributions similar to the observed CHIRPS data, ranging from 1.5 to 2.5 mm/month in the southwest. In the eastern part of the region, the models CNRM-CM6-1-HR, CNRM-CM6-1, AWI-CM-1-1-MR, CMCC-ESM2-1, CESM2-WACCM, and EC-Earth3-C reproduce the rainfall pattern with a range of 3–5 mm/month. However, the ACCESS-CM2 and NorESM2-MM models exhibit a slight reduction in precipitation patterns over the eastern parts. Similarly, the NorESM2-MM, MPI-ESM1-2-HR, and EC-Earth3-C models accurately reproduce the spatial patterns of rainfall in the northern regions. In addition, the EC-Earth3-C, ACCESS-CM2, NorESM2-MM, and CMCC-ESM2-1 models outperform other models in reproducing the spatial trends of rainfall, with a range of 2–3 mm/month, in the central regions. On the other hand, the BCC-CSM2-MR, FGOALS-g3, EC-Earth3-Veg-LR, and CMCC-ESM2 models exhibit inadequate performance in capturing spatial precipitation changes in the central part of the region. This spatial variability in rainfall distribution within the sub-basin primarily arises from the orographic effect and the complex topography (Orke and Li, 2021)

The CMIP6 models were also evaluated for their ability to accurately represent the spatial distribution of mean precipitation in the spring season (SON), using CHIRPS data from 1981 to 2014 (Fig. 5). The results indicated that most of the models successfully captured the annual rainfall variation patterns in the southwestern region. However, the ACCESS-ESM1-5 models exhibited an overestimation of SON rainfall in this area. Three models; MPI-ESM1-2-HR, EC-Earth3, and CNRM-CM6-1-HR - displayed coherent spatial patterns in the central part of the region, with precipitation levels ranging from 4 to 6 mm/month. On the other hand, MPI-ESM1-2-HR, NorESM2-LM, and MIROC underestimated precipitation in the region. CNRM-CM6-1-HR, EC-Earth3, and EC-Earth-C successfully reproduced the spatial patterns of total CHIRPS rainfall in the eastern part of the basin, although there were some differences in precipitation magnitude. Conversely, the EC-Earth3-veg-LR, MIROC, NorESM2-LM, ACCESS-CM2, CMCC-ESM2, CESM2-WACCM, and ACCESS-ESM1-5 models moderately overestimated the amount of SON precipitation in the northern part of the study area, ranging from 6 to 13 mm/month. The highest levels of precipitation (9–14 mm/month) were simulated by ACCESS-ESM1-5 and ACCESS-CM2 in the central region, while the lowest levels (0–3 mm/month) were simulated by MPI-ESM1-2-HR, EC-Earth-C, and NorESM2-LM in the southern region.

The CMIP6 models were also evaluated for their ability to accurately represent the spatial distribution of mean precipitation in the Summer (JJA) and winter season (DJF). The MPI-ESM1-2-HR, EC-Earth3, EC-Earth3-C, CNRM-CM6-1-HR, and MRI-ESM2-0 simulations showed the best performance to capture south eastern parts of JJA precipitation. However, both NESM3, FGOALS-f3-L, MIROC6 ACCESS-ESM1-5, BCC-CSM2-simulation did not well capture central parts of observed precipitation of DJF seasons over the study area, indicating that both somehow overestimated the observed rainfall values. The CNRM-CM6-1-HR, EC-Earth3, EC-Earth3-C, ACCESS-CM2, MPI-ESM1-2-HR simulation data showed capability most parts of sub-basin to represent the summer (JJA) observed values compared to all the other models. Whereas, EC-Earth3-C, EC-Earth3-Veg-LR, MPI-ESM1-2-LR, EC-Earth3-C and EC-Earth3 simulation shows good performance of north, south, eastern, central and western parts of sub-basin during winter season (DJF). Respectively.

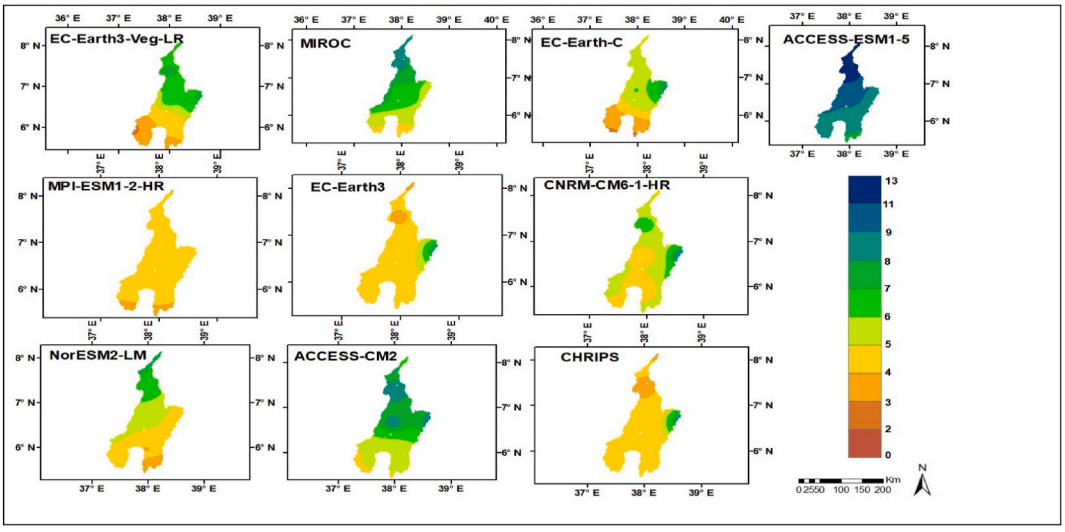


**Fig. 5.** Spatial distribution of mean precipitation during the SON season for 20 CMIP6 models and CHIRPS over the Abaya-Chamo Sub-basin from 1981 to 2014.

### 3.5. Statistical analysis

The normalized root-mean-square error (RMSE), percent bias (PB), and Kling-gupta efficiency (KGE) indices were chosen to visualize the model's performance in relation to the CHIRPS v.2.0 reference datasets (Table 2). To assess the skillfulness of the CMIP6 models, their ability to achieve an optimal bias value of 0, a small NRMSE (<0), and KGE values close to 1 were considered.

Table 2 presents the results which indicate significant variation in performances of most of the CMIP6 models. These models generally demonstrate low to medium levels of acceptable performance based on statistical indices. For example, CESM2-WACCM, EC-Earth3-C, EC-Earth3-Veg-LR, MPI-ESM1-2-HR, and BCC-CSM2-MR show relatively acceptable levels of performance in terms of NSE. EC-Earth3-Veg-LR and EC-Earth3-C accurately represent observed precipitation in the region with NSE values of 0.8 and 0.9 respectively. However, MIROC6, ACCESS-ESM1-5, FGOALS-g3, AWI-CM-1-1-MR, MRI-ESMO-2, and MPI-ESM1-2-LR exhibit relatively unsatisfactory performance in the region. The PB pattern values in the region vary from −144.94 to 41.16, indicating both underestimation and overestimation compared to the observed dataset. EC-Earth3-C and EC-Earth3 models show relatively good performance with low-magnitude PB values of 0.76 and 0.0 respectively. However, MIROC6, ACCESS-ESM1-5, and FGOALS-g3 exhibit high levels of systematic bias, specifically underestimating observed precipitation in the region. These results are consistent with other previous studies over IGAD region of Eastern Africa [7].

The performance of CMIP6 models in terms of normalized root mean square error (NRMSE) - specifically EC-Earth3-C, EC-Earth3, EC-Earth3-Veg-LR, MPI-ESM1-2-HR, and CNRM-ESM2-1 with NRMSE values of 0.33, 0.38, 0.40, 0.5, and 0.59 respectively - indicates favorable results over the region. Conversely, the models MIROC6, ACCESS-ESM1-5, and FGOALS-g3 scored the highest NRMSE values of 4.1, 1.68, and 1.47 respectively, indicating poorer performance compared to the others. In addition to NRMSE, the CMIP6 model performances were evaluated using the Kling-Gupta efficiency (KGE) metric. The top five ranked models based on KGE are EC-Earth-C (0.28), MPI-ESM1-2-HR (0.11), MPI-ESM1-2-LR (0.34), FGOALS-f3-L (0.16), and EC-Earth3-Veg-LR (0.15). However, MIROC6, ACCESS-ESM1-5, MRI-ESMO-2, and NorESM2-LM scored low values of KGE ratio over the region and were unable to accurately simulate annual precipitation patterns.

The evaluation of CMIP6 climate models using monthly observations from CHIRPS for baseline periods revealed that CESM2-WACCM (NSE-0.3), EC-Earth3-C (PB-0.76), EC-Earth3-C (NRMSE-0.33), and EC-Earth-C (KGE-0.28) performed the best in the Abaya-Chamo sub-basin for future climate projections. Individual models exhibited variation in skill within the four indexes analyzed. For example, EC-Earth-C performed well in terms of KGE and NRMSE, but poorly in terms of NSE. Similarly, CESM2-WACCM performed better in NSE, but poorly in PB and KGE. Therefore, selecting a specific model for a given study area based on a single metric is subjective and challenging. Inclusive overall ranking approaches that combine multiple statistical indices are necessary to determine the best performing CMIP6 multi-mean ensemble (MME). This approach increases confidence in model selection and provides insight into the full range of possible future climate changes and associated uncertainties.

### 3.6. Ranking and selection of GCMs

The models were ranked using the Technique for Order Preference by Similarity to the Ideal Solution (TOPSIS). Table 3 presents the ranking of the 20 CMIP6 models over the Abaya-Chamo sub-basin. The model that ranked first is considered the best-performing CMIP6 model. The model that ranked first is considered the best-performing CMIP6 model over others. Among the individual models, EC-Earth3-C outperforms the others. EC-Earth3, EC-Earth3-Veg-LR, ACCESS-CM2, MPI-ESM1-2-HR, and CNRM-CM6-1-HR demonstrate the best performances, displaying good agreement with the baseline period observational datasets. On the other hand,

**Table 2**
Summary statistical indices of CMIP6 model performance for annual scale against CHIRPS data over the Abaya-Chamo Sub-basin during 1981–2014.

| Model | NRMSE | PB | NSE | KGE |
|---|---|---|---|---|
| MPI-ESM1-2-HR | 0.5 | 15.71 | −3.26 | 0.11 |
| MPI-ESM1-2-LR | 0.61 | 22.3 | −5.4 | 0.34 |
| MRI-ESMO-2 | 1.04 | −39.48 | −17.7 | −0.55 |
| NESM3 | 0.59 | 23.11 | −5.14 | −0.06 |
| NorESM2-LM | 0.65 | 17.81 | −6.42 | −0.38 |
| NorESM2-MM | 0.69 | −11.66 | −7.36 | −0.2 |
| ACCESS-CM2 | 0.45 | 12.68 | −2.52 | 0.01 |
| ACCESS-ESM1-5 | 1.68 | −69.96 | −48.04 | −0.84 |
| AWI-CM-1-1-MR | 0.91 | 21.03 | −13.43 | 0 |
| BCC-CSM2-MR | 1.13 | −47.54 | −1.19 | 0.05 |
| CESM2-WACCM | 0.6 | −16.35 | 0.3 | −0.24 |
| CNRM-CM6-1 | 0.61 | 15.21 | −5.47 | −0.29 |
| CNRM-CM6-1-HR | 0.6 | 17.09 | −5.32 | −0.14 |
| CNRM-ESM2-1 | 0.59 | 20.5 | −5.05 | 0.09 |
| EC-Earth3 | 0.38 | 0 | −1.45 | 0.03 |
| EC-Earth3-C | 0.33 | 0.76 | 0.9 | 0.28 |
| EC-Earth3-Veg-LR | 0.4 | −8.51 | 0.8 | 0.15 |
| FGOALS-f3-L | 0.99 | 41.16 | −1 | 0.16 |
| FGOALS-g3 | 1.47 | −63.61 | −36.44 | −0.11 |
| MIROC6 | 4.11 | −144.94 | −292.5 | −8.79 |

**Table 3**
Ranking of the 20 chosen Global climate models (CMIP6) using multi-decision-making methods.

| Model | Rank | Model | Rank |
|---|---|---|---|
| EC-Earth3-C | 1 | MPI-ESM1-2-LR | 11 |
| EC-Earth3 | 2 | NESM3 | 12 |
| EC-Earth3-Veg-LR | 3 | NorESM2-LM | 13 |
| ACCESS-CM2 | 4 | AWI-CM-1-1-MR | 14 |
| MPI-ESM1-2-HR | 5 | FGOALS-f3-L | 15 |
| CNRM-CM6-1-HR | 6 | MRI-ESMO-2 | 16 |
| NorESM2-MM | 7 | BCC-CSM2-MR | 17 |
| CNRM-ESM2-1 | 8 | FGOALS-g3 | 18 |
| CNRM-CM6-1 | 9 | ACCESS-ESM1-5 | 19 |
| CESM2-WACCM | 10 | MIROC6 | 20 |

the MIROC6, ACCESS-ESM1-5, FGOALS-g3, BCC-CSM2-MR, and MRI-ESMO-2 models exhibit relatively poor agreement with the observed datasets. From the above analyses, it is clear that EC-Earth3-C has the most satisfactory values for NSE (0.90), PB (0.76), and NRMSE (0.33), followed by EC-Earth3-Veg (0.58). This findings are consistent with a previous study [28], which reported that EC-EARTH-3 accurately reproduced mean annual precipitation in certain parts of the sub-basin. An ensemble of best-performing models helps in reducing uncertainties among the models. The previous literature reveals no guideline for selecting the maximum number of GCMs in generating the ensemble [65]. Therefore, the first top six GCM models from the Coupled Model Intercomparison Project Phase 6 (CMIP6) GCMs models were finally selected and averaged in an ensemble for future projection of the region's possible climate change scenarios and impact assessments. Therefore, the top ten GCM models from the Coupled Model Intercomparison Project Phase 6 (CMIP6) will be selected and averaged to generate an ensemble for future projections of the region's climate change scenarios and impact assessments.

## 4. conclusions

In this study, we evaluated 20 CMIP6 models in the Abaya-Chamo sub-basin to assess their ability to replicate historical precipitation patterns. We compared the models' performance in reproducing the spatial and temporal distribution of precipitation in the region with the CHIRPS observational datasets. The CMIP6 simulation was evaluated using temporal pattern mapping, trend analysis, statistical analysis, and multiple-criteria decision-making (MCDM) techniques. The analysis of the CHIRPS reference and observed datasets, along with the model simulation pattern, revealed a predominantly bimodal pattern of precipitation in regions with high rainfall. This pattern occurs primarily from mid-spring (MAM) to summer (JJA). However, some models slightly overestimated or underestimated precipitation in different seasons. Nonetheless, the CESM2-WACCM, NorESM2-MM, NorESM2-LM, and NorESM2-LM models performed relatively better than other models in reproducing autumn (SON), winter (DJF), spring (MAM), and summer (JJA) precipitation in the Abaya-Chamo sub-basin, respectively.

Regarding the trend analysis of precipitation distribution, models like NorESM2-MM, NorESM2-LM, MPI-ESM1-2-LR, NESM3, MPI-ESM1-2-LR, CNRM-CM6-1-HR, and CNRM-CM6-1 showed decreasing trends in annual precipitation in the study region. On the other hand, models like BCC-CSM2-MR, FGOALS-g3, EC-Earth3-Veg-LR, EC-Earth3-C, and MPI-ESM1-2-MR displayed positive linear trends in annual precipitation. EC-Earth3-Veg-LR, BCC-CSM2-MR, and AWI-CM-1-1-MR exhibited increasing trends throughout all seasons, which aligned with the observations. CNRM-CM6-1, BCC-CSM2-MR, CNRM-CM6-1, and EC-Earth3-C relatively reproduced the spatial climatological patterns of the observation reference datasets (CHIRPS v2.0) for the MAM season in the southwest, eastern, northern, and central parts of the region, respectively. The overall comparison between the CMIP6 models and CHIRPS, using the normalized root mean square error (NRMS), indicated that the EC-Earth3-C model performed the best with an NRMS of 0.33, followed by EC-Earth3 with an NRMS of 0.58. EC-Earth3-Veg-LR and EC-Earth3-C, with normalized standard error (NSE) values of 0.8 and 0.9 respectively, accurately represented the observed precipitation features in the region. The comprehensive ranking from all the statistical analyses, using the technique for order preferences similar to an ideal solution (TOPSIS) method, indicated that EC-Earth3-C, EC-Earth3, EC-Earth3-Veg-LR, ACCESS-CM2, MPI-ESM1-2-HR, and CNRM-CM6-1-HR performed well in reproducing the precipitation patterns observed during the baseline period.

## Data availability statement

Data used in this study are available from the Ethiopian National Meteorological Agency (NMA) (http://wwwnmsa@ethionet.et) and Earth System Grid Federation (ESGF) archive (https://esgf-node.llnl.gov/search/cmip6/). Meteorological data used to support the study are available from the National Meteorological Agency upon request.

## Funding

This research did not receive any specific external grants from funding Agencies.

## CRediT authorship contribution statement

**Desalegn Laelago Ersado:** Writing – review & editing, Writing – original draft, Methodology, Formal analysis, Data curation, Conceptualization. **Admasu Gebeyehu Awoke:** Supervision.

## Declaration of competing interest

The authors declare that they have no known competing financial interests or personal relationships that could have appeared to influence the work reported in this paper.

## Acknowledgments

The authors acknowledge the Ethiopian National Meteorological Agency (NMA) for meteorological data and the World Climate Research Program (WCRP) Working Group on Coupled Models (WGCM) for making the latest outputs from Coupled Model Intercomparison Project (CMIP) phase six. Corresponding author would like to express sincere gratitude for Addis Ababa University and Hawassa University for supervision and the support to conduct this research.

## Appendix. List of Selected CMIP6 Models

**Table**
The List of employed CMIP6 GCMs pool considered in the present study

| No. | CMIP6 Model Name | Institution | Horizontal Resolution (long lat (Deg) |
|---|---|---|---|
| 1 | BCC-CSM2-MR | Beijing Climate Center, China | 1.13 × 1.13 |
| 2 | EC-Earth3-C | EC-EARTH consortium, Europe | 0.70 × 0.70 |
| 3 | CNRM-CM6-1-HR | Centre National de Recherches M'etéorologiques (CNRM); Centre Europ'een de Recherches et de Formation Avanc'eeen Calcul Scientifique | 0.5 × 0.5 |
| 4 | CESM2-WACCM | National Center for Atmospheric Research, USA | 1.25 × 0.94 |
| 5 | NorESM2-MM | Norwegian Climate Centre/Norway | 1.88 × 2.5 |
| 6 | MIROC6 | National Institute for Environmental Studies, Japan | 1.4 × 1.4 |
| 7 | MPI-ESM1-2-LR | Max Planck Institute for Meteorology (MPI), Germany | 1.88 × 1.88 |
| 8 | MRI-ESM2-0 | Meteorological Research Institute, Japan | 1.13 × 1.13 |
| 9 | CNRM-ESM2-1 | Centre National de Recherches Meteorologiques, Toulouse, France | 1.41 × 1.41 |
| 10 | CNRM-CM6-1 | Centre National de Recherches Météorologiques (CNRM); Centre Européen de Recherches et de Formation Avancéeen Calcul Scientifique, France | 1.41 × 1.41 |
| 11 | NorESM2-LM | Norwegian Climate Center, Norway | 1.88 × 2.5 |
| 12 | EC-Earth3-Veg-LR | EC-EARTH consortium, Europe | 0.70 × 0.70 |
| 13 | ACCESS-CM2 | Common wealth science and industrial research organization, Australia | 1.25 × 1.88 |
| 14 | NESM3 | Nanjing university of information science and technology/china | 1.88 × 1.88 |
| 15 | EC-Earth3 | EC-EARTH consortium, Europe | 0.70 × 0.70 |
| 16 | MPI-ESM1-2-HR | Max Planck Institute for Meteorology (MPI), Germany | 0.9 × 0.9 |
| 17 | AWI-CM-1-1-MR | NOAA Geophysical Fluid Dynamics Laboratory | 1.0 × 1.3 |
| 18 | FGOALS-f3-L | Chinese academy of science, China | 1.3 × 1 |
| 19 | FGOALS-g3 | Chinese academy of science, China | 2.25 × 20 |
| 20 | ACCESS-ESM1-5 | Common wealth science and industrial research organization/Austria | 1.25 × 1.88 |

## References

[1] A.A. Alaminie, S.A. Tilahun, S.A. Legesse, F.A. Zimale, G.B. Tarkegn, M.R. Jury, Evaluation of past and future climate trends under CMIP6 scenarios for the UBNB (abay), Ethiopia, Water 13 (2110) (2021).
[2] D. Mekonnen, B. Hussen, A. Minch, A. Minch, Assessment of climate change impact on flood frequency of bilate river basin , Ethiopia, Civ. Environ. Res. 8 (12) (2016) 27–43.
[3] G. Feyissa, G. Zeleke, W. Bewket, E. Gebremariam, Downscaling of future temperature and precipitation extremes in Addis Ababa under climate change, Water 6 (58) (2018), https://doi.org/10.3390/cli6030058.
[4] A. Shalishe, Evaluation of Climate Change Impacts on Run-Off in the Gidabo River Basin, January, 2017, https://doi.org/10.4172/2573-458X.1000129.
[5] A.S. Shanka, Environment pollution and climate change evaluation of climate change impacts on run-off in the Gidabo river basin : southern Ethiopia, Env. Pollut Clim. Chang. 1 (3) (2017) 1–6, https://doi.org/10.4172/2573-458X.1000129.
[6] Y. Biniyam, A. Kemal, Earth science & climatic change the impacts of climate change on rainfall and flood frequency : the 8 (1) (2017) 1–5, https://doi.org/10.4172/2157-7617.1000383.
[7] P.O. Omay, C. Oludhe, Z. Atheru, Evaluation of CMIP6 historical simulations over IGAD region of eastern Africa, Res. Sq. (2023) 1–27, https://doi.org/10.21203/rs.3.rs-2747422.

[8] V. Eyring, et al., Overview of the Coupled Model Intercomparison Project Phase 6 (CMIP6) Experimental Design and Organization, 2016, pp. 1937–1958, https://doi.org/10.5194/gmd-9-1937-2016.

[9] IPCC, in: T.F. Stocker, D. Qin, G.-K. Plattner, M. Tignor (Eds.), Workshop Report of Intergovernmental Panel on Climate Change Workshop on Regional Climate Projections and Their Use in Impacts and Risk Analysis Studies, IPCC Working Group I Technical Supp, 2015.

[10] M.S. Shiru, Performance evaluation of CMIP6 global climate models for selecting models for climate projection over Nigeria, Theor. Appl. Climatol. 146 (2021) 599–615.

[11] K. Alotaibi, A.R. Ghumman, H. Haider, Y.M. Ghazaw, M. Shafiquzzama, Future predictions of rainfall and temperature using GCM and ann for arid regions : a case study for, Water 10 (1260) (2018), https://doi.org/10.3390/w10091260.

[12] S. Chang, W. Graham, J. Geurink, N. Wanakule, T. Asefa, Evaluation of impacts of future climate change and water use scenarios on regional hydrology, Hydrol. Earth Syst. Sci. 22 (4793) (2018) 4793–4813, https://doi.org/10.5194/hess-22-4793-2018.

[13] Y. Ruan, Z. Yao, R. Wang, Z. Liu, Ranking of CMIP5 GCM skills in simulating observed precipitation over the lower mekong basin, Water 10 (1868) (2018) 1–22, https://doi.org/10.3390/w10121868.

[14] G.T. Gnitou, G. Tan, R. Niu, I.K. Nooni, Assessing past climate biases and the added value of CORDEX-CORE assessing past climate biases and the added value of CORDEX-CORE precipitation simulations over Africa, Remote Sens 13 (2058) (2021), https://doi.org/10.3390/rs13112058.

[15] A. Afolayan, V. Ongoma, G.J. Kooperman, Evaluation of CMIP6 models in simulating the statistics of extreme precipitation over Eastern Africa, Atmos. Res. 254 (November 2020) (2021) 105509, https://doi.org/10.1016/j.atmosres.2021.105509.

[16] B. Ayugi, V. Dike, H. Ngoma, H. Babaousmail, R. Mumo, V. Ongoma, Future changes in precipitation extremes over East Africa based on CMIP6 models, Water 13 (2358) (2021) 1–19.

[17] B. Ayugi, V. Dike, H. Ngoma, H. Babaousmail, R. Mumo, V. Ongoma, Future Changes in Precipitation Extremes over East Africa Based on CMIP6 Future Changes in Precipitation Extremes over East Africa Based on CMIP6 Models, 2021, https://doi.org/10.3390/w13172358. August.

[18] B. Ayugi, G. Tan, G. Tchalim, M. Ojara, V. Ongoma, Historical evaluations and simulations of precipitation over East Africa from Rossby centre regional climate model, Atmos. Res. 232 (October 2019) (2020) 104705, https://doi.org/10.1016/j.atmosres.2019.104705.

[19] M. Mohammed, M.D. Belete, "Hydrological impacts of climate change in tikur wuha watershed , Ethiopian Rift Valley basin hydrological impacts of climate change in tikur wuha watershed, Ethiopian Rift Valley Basin," (September) (2020), https://doi.org/10.7176/JEES/10-2-04.

[20] G.G. Wodaje, Z.E. Asfaw, M.A. Denboba, Impacts and uncertainties of climate change on stream flow of the Bilate River (Ethiopia), using a CMIP5 general circulation models ensemble, Water Resour. Environ. Eng. 13 (1) (2021) 64–75, https://doi.org/10.5897/IJWREE2020.0973.

[21] A.W. Worqlul, Y.T. Dile, E.K. Ayana, J. Jeong, Impact of Climate Change on Streamflow Hydrology in Headwater Catchments of the Upper Blue Nile, 2018, https://doi.org/10.3390/w10020120.

[22] A.G. Shumet, K.T. Mengistu, Assessing the impact of existing and future water demand on economic and environmental aspects (case study from Rift Valley lake basin: meki-ziway sub basin), Ethiopia, Int. J. Waste Resour. 6 (2) (2016), https://doi.org/10.4172/2252-5211.1000223.

[23] A.E. Gebeyehu, Z. Chunju, Z. Yihong, N. Wagasho, Drought event analysis and projection of future precipitation scenario in drought event analysis and projection of future precipitation scenario in Abaya Chamo Sub-Basin , Ethiopia, Eng. Technol. Sci. 51 (5.8) (2019) 707–722, https://doi.org/10.5614/j.eng.technol.sci.2019.51.5.8.

[24] K.S. Raju, D.N. Kumar, "Review of approaches for selection and ensembling of GCMs," (2020) 577–599, https://doi.org/10.2166/wcc.2020.128, no. i.

[25] X. Yang, et al., The optimal multimodel ensemble of bias-corrected CMIP5 climate models over China, HYDROMETEOROLOGY 21 (2020) 845–863, https://doi.org/10.1175/JHM-D-19-0141.1.

[26] H. Babaousmail, et al., Evaluation of the performance of CMIP6 models in reproducing rainfall patterns over North Africa, Atmosphere 12 (475) (2021) 1–25.

[27] S.H. Gebresellase, Evaluation of CMIP6 climate models for climate change impact assessments in upper Awash, 0–41, Res. J. Appl. Sci. Eng. Technol. (2022), https://doi.org/10.21203/rs.3.rs-1231424.

[28] R. Girma, C. Fürst, A. Moges, Performance evaluation of CORDEX-Africa regional climate models in simulating climate variables over Ethiopian main rift valley: evidence from Gidabo river basin for impact modeling studies, Dyn. Atmos. Ocean. 99 (101317) (2022) 3–4, https://doi.org/10.1016/j.dynatmoce.2022.101317.

[29] T.A. Feyissa, T.A. Demissie, F. Saathoff, Evaluation of general circulation models CMIP6 performance and future climate change over the Omo river basin , Ethiopia, MDPI,Sustainability 2023 15 (6507) (2023).

[30] C.H. Sime, W.T. Dibaba, Evaluation of CMIP6 model performance and extreme precipitation prediction in the Awash basin, Heliyon 9 (11) (2023) e21578, https://doi.org/10.1016/j.heliyon.2023.e21578.

[31] D. Berhanu, T. Alamirew, M.T. Taye, D. Tibebe, S. Gebrehiwota, G. Zeleke, Evaluation of CMIP6 models in reproducing observed rainfall over Ethiopia, Water Clim. Chang. 00 (0) (2023) 1–22, https://doi.org/10.2166/wcc.2023.502.

[32] S.K. Balcha, T.A. Hulluka, A.A. Awass, A. Bantider, Performance evaluation of multiple regional climate models to simulate rainfall in the Central Rift Valley Lakes Basin of Ethiopia and their selection criteria for the best climate model, Env. Monit Assess 195 (888) (2023), https://doi.org/10.1007/s10661-023-11437-w.

[33] H.G. Kuma, Hydrologic responses to climate and land-use/land-cover changes in the Bilate, Water Clim. Chang. 12 (8) (2021) 3750–3769, https://doi.org/10.2166/wcc.2021.281.

[34] S.K. Balcha, Assessment of future climate change impact on water balance components in Central Rift Valley Lakes Basin , Ethiopia, Water Clim. Chang. 14 (1) (2023) 175–199, https://doi.org/10.2166/wcc.2022.249.

[35] E.E. Temesgen, D.A. Areru, Arba, D. Wendemeneh, The impact of climate change on the Rift-VALLEY LAKES basin in southern Ethiopia : a review, J. Digit. Food, Energy Water Syst. 3 (1) (2022) 1–15.

[36] B. Hussen, N. Wagesho, Regional flood frequency analysis for Abaya – Chamo Sub-Basin, Rift Valley basin Ethiopia, J. Resour. Dev. Manag. 24 (January) (2016) 15–28.

[37] A.E. Gebeyehu, Z. Chunju, Z. Yihong, Assessment and mapping of land use change by remote sensing and GIS: a Case Study of Abaya Chamo Sub-basin, Ethiopia, Nat. Environ. Pollut. Technol. 18 (2) (2019) 549–554.

[38] A.W. Yohannes, M. Cotter, G. Kelboro, W. Dessalegn, Land use and land cover changes and their effects on the landscape of Abaya-Chamo basin, Southern Ethiopia, Land 7 (1) (2018), https://doi.org/10.3390/land7010002.

[39] K. Ahmed, Modeling Climate Change Impacts on Precipitation in Arid Regions of Pakistan : a Non-local Model Output Statistics Downscaling Approach, 2018.

[40] W. Norliyana, W. Ismail, W. Zawiah, W. Zin, W. Ibrahim, Estimation of rainfall and stream flow missing data for Terengganu , Malaysia by using interpolation technique methods 13 (3) (2017) 213–217.

[41] S. Gleixner, T. Demissie, G.T. Diro, Did ERA5 Improve Temperature and Precipitation Reanalysis over East Africa ?, 2020, pp. 1–19, https://doi.org/10.3390/atmos11090996.

[42] Q. Hu, Z. Li, L. Wang, Y. Huang, Y. Wang, L. Li, Rainfall Spatial Estimations : A Review from Spatial Interpolation to Multi-Source Data Merging, MDPI, 2019, pp. 1–30, https://doi.org/10.3390/w11030579.

[43] G. Dubache, B. Asmerom, W. Ullah, B. Alex, O. Farshad, A. Zhu, Testing the accuracy of high - resolution satellite - based and numerical model output precipitation products over Ethiopia, Theor. Appl. Climatol. (2021) 1127–1142, https://doi.org/10.1007/s00704-021-03783-x.

[44] K. Teshome, Comparison of high-resolution satellite based rainfall products at basin scale : the case of omo-gibe river basin , Ethiopia, World Sci. News 165 (2022) 110–129.

[45] A.T. Hordofa, O.T. Leta, T. Alamirew, N.S. Kawo, A.D. Chukalla, Performance evaluation and comparison of satellite-derived rainfall datasets over the ziway lake basin , Ethiopia, Climate 9 (113) (2021), https://doi.org/10.3390/cli9070113.

[46] Uwe Schulzweida, CDO User Guide, October. 2021.

[47] S. Roy, Rainfall analysis by using mann-kendall trend , sen ' s slope and variability at six stations of andaman & nicobar islands, Res. J. Appl. Sci. Eng. Technol. (2021).

[48] M. Gocic, S. Trajkovic, Analysis of changes in meteorological variables using Mann-Kendall and Sen ' s slope estimator statistical tests in Serbia, Glob. Planet. Change 100 (2013) 172–182, https://doi.org/10.1016/j.gloplacha.2012.10.014.
[49] M.S. Madhusudhan, H.J. Ningaraju, M.R. Shashank Patil, Analysis of rainfall trend series using Mann- Kendall and Sen's slope estimator statistical test in mandya district, Karnataka, Int. Res. J. Eng. Technol. 8 (5) (2021) 3387–3393.
[50] A. Bouklikha, M. Habi, A. Elouissi, S. Hamoudi, Annual, seasonal and monthly rainfall trend analysis in the Tafna watershed, Algeria, Appl. Water Sci. 11 (4) (2021) 1–21, https://doi.org/10.1007/s13201-021-01404-6.
[51] T.M. Weldegerima, T.T. Zeleke, B.S. Birhanu, B.F. Zaitchik, Z.A. Fetene, Analysis of rainfall trends and its relationship with SST signals in the lake tana basin , Ethiopia, Hindawi Adv. Meteorol. (2018), https://doi.org/10.1155/2018/5869010.
[52] J. Li, R. Huo, H. Chen, Y. Zhao, T. Zhao, Comparative assessment and future prediction using CMIP6 and CMIP5 for annual precipitation and extreme precipitation simulation, Front. Earth Sci. 9 (June) (2021) 1–20, https://doi.org/10.3389/feart.2021.687976.
[53] P. Anttila, T. Ruoho-airola, Detecting Trends of Annual Values of Atmospheric Pollutants by the Mann- Kendall Test and Sen ' S Solpe Estimates the Excel Template Application MAKESENS, vol. 31, January. 2002.
[54] H. Jiqin, F.T. Gelata, Application of MK trend and test of Sen ' s slope estimator to measure impact of climate change on the adoption of conservation agriculture in Ethiopia, Water Clim. Chang. 14 (3) (2023) 977–988, https://doi.org/10.2166/wcc.2023.508.
[55] P.K. Sen, Estimates of the regression coefficient based on kendall's tau, J. Am. Stat. Assoc. 63 (324) (1968) 1379–1389, https://doi.org/10.1080/01621459.1968.10480934.
[56] M.S. Nashwan, A Novel Framework for Selecting General Circulation Models Based on the Spatial Patterns of Climate, January, 2020, https://doi.org/10.1002/joc.6465.
[57] N.R. Hounguè, A.D.S. Almoradie, M. Evers, A multi criteria decision analysis approach for regional climate model selection and future climate assessment in the mono river basin, Benin and Togo, Atmosphere 13 (9) (2022), https://doi.org/10.3390/atmos13091471.
[58] M.L. Edamo, et al., A comparative assessment of multi-criteria decision-making analysis and machine learning methods for flood susceptibility mapping and socio-economic impacts on flood risk in Abela-Abaya floodplain of Ethiopia, Environ. Challenges 9 (2022) 100629, https://doi.org/10.1016/j.envc.2022.100629.
[59] A.M. Melesse, W. Abtew, S.G. Setegn, Nile River Basin: ecohydrological challenges, climate change and hydropolitics, Nile River Basin Ecohydrol. Challenges, Clim. Chang. Hydropolitics (June 2018) (2013) 1–718, https://doi.org/10.1007/978-3-319-02720-3.
[60] C. Mcsweeney, M. New, G. Lizcano, UNDP Climate Change Country Profiles, Ethiopia, 2016.
[61] A.E. Gebeyehu, Z. Chunju, Z. Yihong, N. Wagasho, Drought event analysis and projection of future precipitation scenario in Abaya Chamo sub-basin, Ethiopia, J. Eng. Technol. Sci. 51 (5) (2019) 707–728, https://doi.org/10.5614/j.eng.technol.sci.2019.51.5.8.
[62] A. Alhamshry, A.A. Fenta, H. Yasuda, R. Kimura, K. Shimizu, Seasonal rainfall variability in Ethiopia and its long-term link to global sea surface temperatures, water 12 (55) (2020) 1–19, https://doi.org/10.3390/w12010055.
[63] A. Belay, et al., Analysis of climate variability and trends in southern Ethiopia, Climate 9 (96) (2021) 1–17, https://doi.org/10.3390/cli9060096.
[64] Y.A. Orke, M. Li, Hydroclimatic variability in the bilate watershed, Ethiopia, Climate 9 (98) (2021), https://doi.org/10.3390/cli9060096.
[65] H. Ngoma, W. Wen, B. Ayugi, R. Karim, V. Ongoma, Evaluation of precipitation simulations in CMIP6 models over Uganda, Int J Clim (2021) 1–26, https://doi.org/10.1002/joc.7098.